J. Water Environ. Nanotechnol., 9(2): 149-172 Spring 2024

ORIGINAL RESEARCH PAPER

Highly Efficient Scavenging of Nitrophenol, Arsenic (V), Copper (II), Dibenzothiphene, and Carbazole by Nanoporous Silica/Carbon Adsorbents for Remediation of Oil and Water Pollutants

Ghasem Zolfaghari*

Department of Environmental Sciences and Engineering, Faculty of Environmental Sciences, Hakim Sabzevari University, Razavi Khorasan, Sabzevar, P.O. Box: 397, Iran

Received: 2023-11-22 Accepted: 2024-01-15 Published: 2024-05-12

ABSTRACT

In the present study, the removal of *p*-nitrophenol (PNP) by a newly designed mesoporous organocarbon, monolayers of ß-cyclodextrin (CD) on oxidized ordered nanoporous carbon (OX-ONC) via 1,4-phenylene diisocyanate (PDI) linking denoted as CD-ONC was optimized. Furthermore, Au-doped mesoporous carbon CMK-3 denoted as Au-OCMK-3 was synthesized by using SBA-15. Au-OCMK-3 has been studied for the removal of dibenzothiophene (DBT) and carbazole (CA) from *n*-hexane. Also, the functionalization of SBA-16 mesoporous with sulfonic acid for arsenic (As (V)) and copper (Cu (II)) removal was carried out (SBA-16-SO_3H). The maximum absorption capacity of CD-ONC was 100 mg/g. Dubinin–Radushkevich isotherm was applied to describe the nature of PNP uptake and it was found that it occurred physically (*E* = 0.07 KJ/mol, CD-ONC). The value for Temkin's heat of adsorption is positive for PNP (157.87 J/mol, CD-ONC). There are two physisorption models of PNP with the surface C=O groups of ONC (H-bond and dispersion effect between phenolic ring and π electrons). The overall PNP adsorption process was exothermic and spontaneous according to thermodynamics parameters (free energy (ΔG^o), enthalpy (ΔH^o), and entropy (ΔS^o)). We demonstrate that functionalization of CMK-3 with gold is possible (q_m value for DBT: 15.33 mg/g and for CA: 13.00 mg/g). The adsorption capacity for As (V) on SBA-16- SO_3H reaches 92.63 mg/g. The high removal of As equilibrium time of 90 minutes can be explained in terms of a strong electrostatic attraction that occurred between the SO_3H and As. Maximum absorption capacity was 92.63 mg/g for As(V) and 13.00 mg/g for Cu(II).

Keywords: *Ligands-bridged mesoporous, Taguchi method, Response Surface Methodology, Organic pollutants, Inorganic pollutants*

How to cite this article

Zolfaghari G., Highly Efficient Scavenging of Nitrophenol, Arsenic (V), Copper (II), Dibenzothiphene, and Carbazole by Nanoporous Silica/Carbon Adsorbents for Remediation of Oil and Water Pollutants. J. Water Environ. Nanotechnol., 2024; 9(2): 149-172. DOI: 10.22090/jwent.2024.02.03

INTRODUCTION

Various substances and materials are generated through industrial processes that can contaminate waters, which will negatively affect the environment and humans [1-4]. Phenols, due to being toxic even at low concentrations, are among the most common organic water pollutants [5]. The maximum concentration of phenol in drinking water is determined as 0.001 mg/L by WHO (1963). The *p*-nitrophenol (PNP) and its derivatives, usually found in the wastewater from dyes, textile, pesticides, plasticizers, and herbicides industries are all toxic and refractory pollutants [6]. Numerous physicochemical treatment technologies and materials have been used to decompose PNP and improve its biodegradation, including activated carbon, clay, Fenton reagent, nanosized nickel catalysts, ultrasound enhanced, and sonophotocatalytic process [7,8]. There are

* Corresponding Authors Email: *ghr_zolfaghari@yahoo.com, g.zolfaghari@hsu.ac.ir*

alternative adsorbents such as biosorbents [9] zeolites [10] and resins [11]. However, at high concentrations of PNP and long purification times, these methods have disadvantages and limitations. There is a large amount of organic sulfur compounds with a concentration of 300 and 500 ppm in commercial gasoline and diesel [12]. The sulfur compounds in oil can cause serious environmental problems by converting into SO_x compounds during combustion. Thus, the desulfurization process appears to be a necessary procedure throughout the world, which has turned into a major unit operation in petroleum refining [13]. Dibenzothiophene (DBT) is a refractory species. In addition, due to the low reactivity rates, nitrogen-containing compounds such as carbazole act as inhibitors in various refinery processes. Arsenic compounds can cause short-term and long-term effects in humans, plants, and animals. The affected areas have arsenic levels much higher than the maximum allowed contamination level (0.01 mg/L). The treatment of arsenic contamination is of irrefutable significance to lower floras and faunas, humanity, and their living ecosystem. Numerous technologies and materials have been used to decompose arsenic including adsorption, ion exchanges, electrokinetic processes, electrocoagulation, chemical precipitation, phytoremediation, membrane technology, and phytobial remediation [14]. Copper is required for humans, but if it exceeds the permissible limit, it causes many problems. In human beings, the major source of exposure to copper is via water that reaches through irrigation and underground water resources. Copper poisoning is referred to as "Copperiedus". Gastric hemorrhage leading to evident paralysis and eventually death is one of the most common impacts of copper ingestion. Apart from that, exposure to skin leads to acute dermatitis in human beings [15]. According to the EPA, about 1.3 mg/L of Cu^{2+} ion in industrial sewages is permitted [16]. The biosorption process is useful in copper removal by employing the techniques of adsorption and precipitation [15].

Various methods have been used to remove environmental pollutants [17, 18]. Nanoparticles have been used as adsorbents to remove pollutants in various studies [19, 20, 21, 22]. Adsorption of pollutants by nanomaterials is a critical process in water and wastewater treatment. Due to their special properties, including high surface areas, regular frameworks, and narrow pore size distributions, ordered mesoporous silica (OMC) like MCM-48, Santa Barbara Amorphous-15 (SBA-15) and SBA-16 have been considered by researchers. SBA-15 is a highly stable mesoporous silica sieve developed by researchers at the University of California at Santa Barbara. It gets its high hydrothermal and mechanical stability from a framework of uniform hexagonal pores that feature a narrow pore-size distribution and a tunable pore diameter of 5nm to 15nm. Ordered nanoporous carbons (ONC) can be synthesized by using OMS materials as hard templates. For example, MCM-48 mesoporous silica template leads to CMK-1 carbon [23] and CMK-4 [24]. Mesoporous carbon materials, which possess high surface area, large pore volume, and special physicochemical properties, have caused considerable attention in various fields. These features of mesoporous carbon not only provide a huge interface and large space to accommodate capacious guest species but also enable the specific binding, enrichment, and separation, meeting the requirements of excellent adsorbents. The SBA-15 template with the 2-dimensional (2-D) hexagonal structure is used to synthesize CMK-3 (rod-type framework) [25] and CMK-5 (tube-type) carbons [26].

The syntheses of ordered mesoporous solids are classified as endo template methods ("soft-matter templating"). In exo template methods ("nanocasting"), a porous solid is used as the template in place of the surfactant. Thus, this method is also known as "hard-matter templating". The hollow spaces that provide the exo template framework are filled with an inorganic precursor, which is then transformed (cured) under suitable conditions. In this way, the pore system of the template is copied as a "negative image". After the removal of the now-filled exo template framework, the incorporated material is obtained with a large specific surface area. In a process called hard templating, carbon mesoporous can be produced by using silicate mesoporous as a hard mold and a carbon source (for example, sucrose).

Mesoporous silica particles have great potential as adsorbents due to the intrinsic merits of having a large BET surface area, high porosity, and controllable and narrowly distributed pore sizes. Using modified carbon nanoporous adsorbent, Zolfaghari et al. 2013[27] studied the adsorption of lead from water. Surface functionalization

of porous carbon materials is essential for changing the hydrophobicity and hydrophilicity characteristics of the materials' surface, making them available as proper adsorbents [28]. Cyclodextrins (CDs) as useful materials for functionalization are called Schardinger's dextrins or cycloamyloses, which consist of 6, 7, and 8 glucopyranose units called as α-, ß-, γ-CD [29].

In this study, highly ordered mesoporous carbon molecular sieves, ß-cyclodextrin (CD) on oxidized ordered nanoporous carbon (OX-ONC) via 1,4-phenylene diisocyanate (PDI) linking was synthesized to examine the adsorption of *p*-nitrophenols. Modification of carbon nanoporous with cyclodextrin is an innovative aspect of this study. To optimize the design parameters, the Taguchi robust design method has been modified since this systematic approach is capable of considerably minimizing the overall testing time and the experimental costs [30, 31]. SBA-15 was used as a hard template to prepare the CMK-3, while sucrose was used as the carbon source. Furthermore, CMK-3 was modified with HNO_3 and functionalized with gold solution by a post-synthesis treatment. The Au-doped oxidized mesoporous carbon (Au-OCMK-3) was examined for the removal of dibenzothiophene and carbazole (CA) from the oil model. In addition, the SBA-16 mesoporous silica functionalized with thiol groups and oxidized the thiol to sulfonic acid groups. The nanostructure of SO_3H-SBA-16 was used to remove As (V) and Cu (II) from water. To optimize the adsorption conditions of copper on SO_3H-SBA-16, the Response Surface Methodology (RSM) has been used. In general, the feasibility of using modified nanoporous to remove pollutants is one of the main goals of this research, which has synthesized and modified several different mesoporous adsorbents and examined different conditions for removing pollutants.

TAGUCHI ROBUST DESIGN METHOD

Taguchi's robust design method [31, 32] was introduced in this paper to optimize the controllable factors of pollutant removal efficiency (PRE). Taguchi method uses orthogonal arrays (OAs) of experimental design theory to study a large number of variables with a small number of experiments [33]. Variability is a characteristic of the noise factor, which is difficult to control. Conversely, a factor that is easily controlled is called a control factor. The variability can be expressed by signal-to-noise (S/N) ratio. The experimental condition having the maximum S/N ratio is considered the optimal condition, as the variability of characteristics is in inverse proportion to the S/N ratio [34].

EXPERIMENTAL

Immobilization of β-cyclodextrin on nanoporous

1. Preparation of siliceous template (SBA-16)

We synthesized SBA-16 based on the instructions of other references [35]. We dissolved two poly(alkylene oxide)- type triblock copolymers, P123 and F127 together in the aqueous HCl solution. We then added tetraethoxysilane (TEOS) to the solution and the process of stirring with the magnet was continued.

2. Synthesis of ordered nanoporous carbon (ONC)

The ordered nanoporous carbon was synthesized based on scientific references [36, 37].

3. *Oxidation of ONC (OX-ONC)*

The surface chemistry and texture of ONC by nitric acid (69%, Merck) were modified [38, 39]. First, 0.1 g of dried ONC powder was treated with 15 ml of HNO_3 solution (2 M) for 1 h at 80 ºC under refluxing. After oxidation, the samples were recovered and washed with DW until reaching pH 7.

4. Monolayers of cyclodextrin on ordered nanoporous carbon (CD-ONC)

An amount of 1.0 g of OX-ONC was dried overnight at 125 °C and added into a round bottom flask containing 1,4-phenylene diisocyanate (PDI) (0.336 g). Under an inert Ar atmosphere, the N, N˙-dimethyl formamide (DMF) was added to the mixture, and the reaction vessel was stirred at 70 °C for 8 h. Then 50 ml of β-CD dissolved in the DMF was added dropwise to the reactor over one hour and stirred for 36 hours. The resulting mixture was washed with methanol for 48 hours in a soxhlet extraction process and then vacuum dried overnight at 60 °C. The final product was called CD-ONC.

Immobilization of gold on nanoporous

1. Preparation of SBA-15

The synthesis of SBA-15 was carried out according to the method mentioned by Colilla et al. [40].

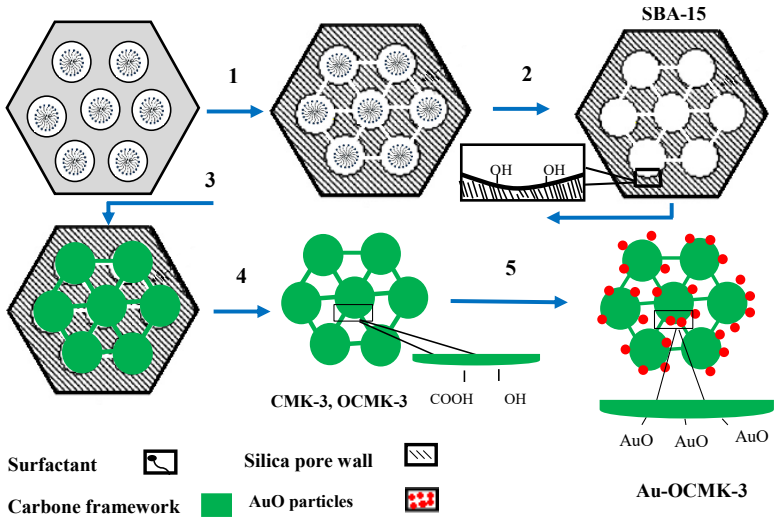

Scheme 1. Preparation strategy of Au-doped mesoporous carbon: (1) the silica introduction into the surfactant; (2) removal of the surfactant template; (3) the carbon source introduction into the ordered mesoporous silica; (4) removal of the silica (CMK-3) and modification with acid (OCMK-3); and (5) Au-doped mesoporous carbon (Au-OCMK-3).

2. Synthesis and oxidation of CMK-3 (OCMK-3)

The synthesis of CMK-3 was carried out according to the method mentioned by Jun et al. [41]. We used nitric acid to oxidize the CMK-3 as described in section 3.1.3.

3. Au-doped mesoporous carbon (Au-OCMK-3)

Au-doped OCMK-3 was prepared by mixing 5000 ppm of $HAuCl_4$ and OCMK-3 for 10 h. The solid was separated by filtration, washed, and vacuum-dried. These samples were reduced to form nanoparticles of Au using 0.1 M $NaBH_4$ solution. Au-doped oxidized mesoporous carbon was studied as a nano absorbent for the removal of dibenzothiophene and carbazole from non-aqueous solutions. The product was denoted as Au-OCMK-3. Scheme 1. shows the preparation strategy of Au-OCMK-3.

Functionalization of SBA-16 with sulfonic acid groups

1. Thiol-functionalized SBA-16 materials (SH-SBA-16)

A value of 0.2 g SBA-15 was dissolved in 20 g 0.1 M HCl aqueous solutions, followed by the addition of 3-mercaptopropyltrimethoxysilane (MPTMS) (molar ratios of MPTMS/SiO_2 = 0.13:1). Stirred for 7 h at the ambient temperature, the mixture was transferred into an autoclave and statically treated for 24 h at 100 °C. As described above, the solid products were then recovered.

2. Oxidation of thiol to sulfonic acid groups (SO_3H-SBA-16)

First, 0.15 g SH-SBA-16 was dissolved in 20 g 2M HCl aqueous solutions, followed by the addition of 0.75 g 30 wt% H_2O_2. Stirred for 5 min at an ambient temperature, the mixture was transferred into an autoclave and statically treated for 6 h at 100 °C. As described above, the solid products were recovered [42]. The product was referred to as SO_3H-SBA-16. Scheme 2. shows the preparation strategy of SBA-16, modification with the thiol group, and functionalization with SO_3H-SBA-16.

Characterization methods

We recorded the X-ray powder diffraction (XRD) patterns on a Philips 1830 diffractometer (in the 2θ range of 1–10). We measured nitrogen adsorption-desorption isotherms of the synthesized samples at 77 K on the Micromeritics model ASAP 2010 absorptiometer [43]. The surface area of the sample was also measured by the Brunaure-Emmet-Teller (BET) method. The morphology (SEM images) of the samples was examined using JEOL 6300F SEM. Raman spectra were obtained using an Almega Thermo Nicolet Dispersive Raman Spectrometer with a resolution (= λ/2) of 0.257 μm (laser spot size).

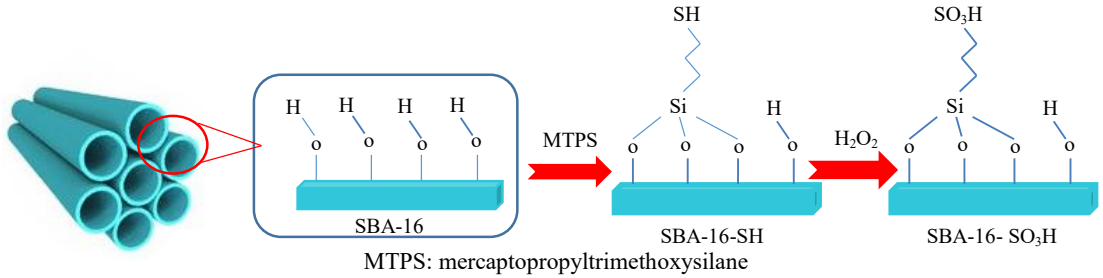

Scheme 2. Preparation strategy of SBA-16; modification with thiol group; and functionalization with SO_3H-SBA-16.

Orthogonal array and experimental parameters

The S/N ratios were different according to the type of characteristic. Our main goal in the research design was to maximize the PRE, as the larger-the-better was required, as shown in Eq. (1):

$$\frac{S}{N} = -10log_{10}\left[\frac{1}{n}\sum\left(\frac{1}{PRE_i}\right)^2\right] \quad (1)$$

In Eq. (1), n is the number of repetitions under the same experimental conditions, while PRE represents the measurements result (pollutant removal efficiency). The orthogonal array of the $L16$ (4^5) type was used. L and subscript 16 denote the Latin square and the repetition number of the experiment, respectively. A series of aqueous solutions of *p*-nitrophenol with an initial concentration of 50-200 mg/L, a temperature of 20-80 °C, a dose of 0.3-0.9 g/L, pH of 2- 10, and an agitation time of 60-240 were prepared. Eq. (2) was used to calculate the pollutant removal efficiency (PRE):

$$PRE = \frac{(C_0 - C_e)}{C_0} \times 100 \quad (2)$$

where C_0 and C_e are the initial and equilibrium concentrations of solute (mg/L), respectively. Based on selection of the five factors with the four levels, the full factorial of this process has been calculated as Eq. (3):

$N=L^m$

where N is the number of possible designs, L number of levels for each factor and m is the number of factors. For this study N is 1024 (4^5) tests. In contrast, in Taguchi method chooses only 16 tests. Other tests based on these S/N ratios can be predicted as Eq. (4) [44]:

$$\left(\frac{S}{N}\right)_P = \left(\frac{S}{N}\right)_m + \sum_{i=1}^{n}\left[\left(\frac{S}{N}\right)_i - \left(\frac{S}{N}\right)_m\right] \quad (4)$$

where $(S/N)_m$ is the total mean S/N ratio, $(S/N)_i$ is the mean S/N ratio at the predicted level, and n is the number of the main design parameters.

Adsorption studies

Table 1 shows some of the characteristics of pollutants being investigated. Distilled water has been used as a solvent for the preparation of *p*-nitrophenol, arsenic (V), and copper (II) solution (aqueous solution). We added 100 ml of *p*-nitrophenol solution with concentrations of 50, 100, 150, and 200 mg/L to a flask and mixed them with 0.09 g (0.9 g/L) of mesoporous carbons (OX-ONC and CD-ONC). The experiments were performed using a stirrer at 150 rpm, 25 °C, 180 min contact time, and pH 6. Hydrochloric acid and sodium hydroxide were used to control the pH and a digital pH-meter device was used to measure the pH (Metrohm, model 654). *p*-Nitrophenol concentration was measured using a UV-Vis Array Spectrophotometer (Photonix Ar 2015, Teifsanje Pishro Pajohesh Company, Iran) and to reduce the measurement error, each experiment was repeated three times. In these experiments, based on the standard calibration curve, a coefficient square (R^2) of 0.99 was obtained. Carbazole and dibenzothiophene were removed with the Au-OCMK-3 at room temperature and contact times of 30, 60, 120, 180, and 240 min, and then a UV-Vis Spectrophotometer was used to measure the removal efficiency of these contaminants. In this study, n-heptane was used as a fuel model, which is a non-aqueous solution. The concentrations of pollutants were determined in the residual solution

Table 1:The physicochemical properties of the studied pollutants.

Pollutant	Molecular formula	Molecular Weight (g/mol)	Melting point (°C)	Boiling point (°C)	Solubility in water
P-nitrophenol	$C_6H_5No_3$	139	113	279	Soluble
Dibenothiophene	$C_{12}H_8S$	184.26	97 to 100	332 to 333	Insoluble
Carbazole	$C_{12}H_9N$	167.211	246.3	354.69	Insoluble
Arsenic	As	74.92	816.8	613	Soluble
Copper	Cu	63.5	1084.62	2562	Soluble

and the amount of adsorption at equilibrium, qe (mg/g) was calculated by Eq. (5):

$$q_e = \frac{(C_0 - C_e)V}{W} \quad (5)$$

where C_0 and C_e (mg/g) are the initial and equilibrium liquid phase concentrations of PNP, respectively; V is the volume of the solution (L), and W is the mass of dry adsorbent used (g) [45]. The adsorption of arsenic on SO_3H-SBA-16 was done at room temperature with the adsorption times of 30, 45, 60, 90, and 120 min. Arsenic stock solutions were prepared by dissolving sodium arsenate (Na_3AsO_4) in degassed pure water with a conductivity of 18 MΩcm. We determined the arsenic content in the samples by an internally accredited and validated Graphite Furnace Atomic Absorption Spectroscopy (GF-AAS) method. We used an Atomic Absorption Spectrometer GBC Scientific Equipment Ltd. coupled with a graphite furnace GF 3000. For copper (II) ion, a solution with a concentration of 500 mg/L was prepared by dissolving appropriate amounts of copper chloride salt in distilled water. To investigate the factors involved in the process of copper adsorption, 0.1 g of the synthesized adsorbent (SO_3H-SBA-16) with 100 mL of copper solutions with concentrations of 10, 20, 30 and 40 mg/L by a mechanical stirrer was stirred at a speed of 150 rpm. The copper concentration was measured using a UV-Vis Array Spectrophotometer at a maximum wavelength of 260 nm. The Response Surface Methodology is a set of statistical techniques used in the optimization of processes where the desired response is affected by several variables. By selecting five factors including temperature, pH, dose, pollutant concentration, and contact time, their simultaneous role in copper removal rate was investigated in a plan consisting of 32 experiments using Design Expert software. Adsorbent dose between 0.2 and 1 g/L, pH between 2 and 8, concentration between 10 and 40 mg/L, temperature between 20 and 35 °C, and contact time between 15 and 90 minutes were considered.

RESULTS AND DISCUSSION

Characterization of synthesized nanomaterials

1. XRD patterns

The XRD patterns of SBA-16, ONC, OX-ONC, and CD-ONC samples are shown in Fig. 1A. The XRD pattern synthesized SBA-16 shows two strong peaks in the 2θ of 0.50 and 1.28, and one weaker reflection at 2θ value 1.40. The body-centered cubic structure, which is represented by (110), (200), and (211) reflections (corresponding to a cubic structure [36], exists in the synthesized SBA-16 sample. The XRD patterns show well-resolved reflections indicating that ordered nanoporous carbon nicely maintains its original structure even after the oxidation and β-cyclodextrin grafting [41]. The XRD patterns of SH-SBA-16 and SO_3H-SBA-16 samples are shown in Fig. 1B.

2. Nitrogen adsorption-desorption technique

After modification with nitric acid and functionalization with cyclodextrin, the obtained carbon retained isotherms type IV. This indicates that all the synthesized materials are mesoporous [46, 47, 48]. As can be seen in Table 2, OX-ONC has a lower surface area than ONC. The reason is the presence of carboxylic groups on the surface of OX-ONC. After the functionalization of the carbon cavities, the surface area and the pore volume of the functionalized carbons with cyclodextrin are reduced. The BET surface area and pore volume of CMK-3 and Au-OCMK-3 were calculated, which are shown in Table 2. It is expected that the gold ions adsorbed on the carbon surface will bond with the mesoporous

Table 2: The results of nitrogen porosimetry measurements.

Nanostructure	Surface Area (m^2/g)	Pore volume (cm^3/g)	Pore size (nm)
ONC	1100	1.60	4.5
OX-ONC	950	1.45	4.1
CD-ONC	890	1.35	5.1
CMK-3	705	0.71	3.8
Au-OCMK-3	914	0.60	3.4

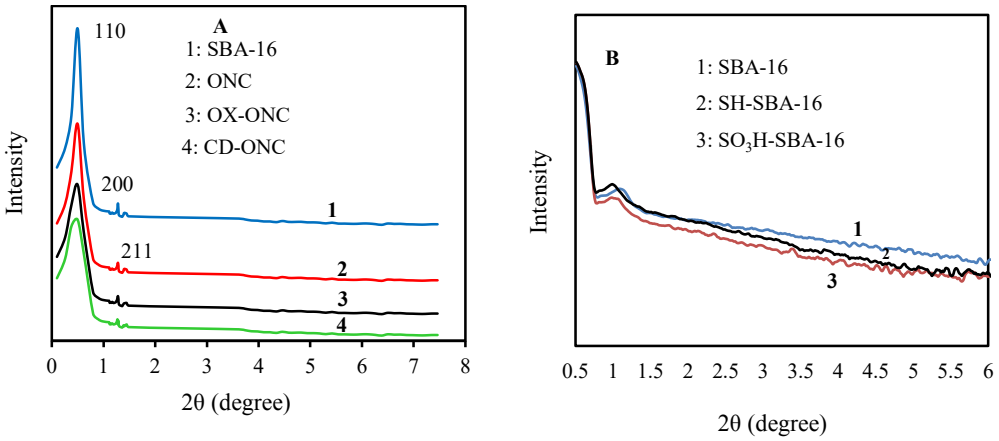

Fig. 1. A) XRD patterns of SBA-16, ONC, OX-ONC, and CD-ONC, and B) XRD patterns of SH-SBA-16 and SO3H-SBA-16.

carbon through oxygen atoms. In this case, the surface area of Au-OCMK-3 may progressively enhance (914 m^2/g) [49].

3. SEM/EDX analysis of nano adsorbents

The SEM image of ordered mesoporous carbon is shown in Fig. 2A. The cage-like ordered mesoporous carbon has a cubic structure with a body-centered-cubic arrangement of cages with 8 apertures to the nearest neighbors as in the SBA-16 [50]. The morphology of ONC was preserved after oxidation and cyclodextrin functionalization (Fig. 3B). Fig. 2C shows the image of Au-OCMK-3; the carbon replica appears to have a wheat-like shape identical to the SBA-15. After oxidation and functionalization with gold, the CMK-3 morphology was preserved. After MPTMS grafting and oxidation of thiol to sulfonic acid groups (SO_3H-SBA-16), the morphology of SBA-16 was preserved as seen in Fig. 2D. The energy dispersive X-ray spectroscopy (EDX) analysis of SBA-16 and SO_3H-SBA-16 is shown in Fig. 2 (E and F). EDS, EDX, EDXS, or XEDS is an analytical method for chemical identification of samples. In this Fig., a peak of sulfur (S) corresponding to SO_3H-SBA-16 can be seen. It is also possible to see the peak of carbon (C) which is caused by $CH_2CH_2CH_2SH$ groups.

4. Raman spectroscopy

In this study, the Raman spectroscopy technique was used to investigate the surface of mesoporous carbons (Fig. 3). As seen in Fig. 3A, regular nanoporous carbon has three D (1337 cm^{-1}), G (1599 cm^{-1}), and D+G bands (2935 cm^{-1}). These bands are characterized by different structures and stretching modes. The vibration at 1337 cm^{-1} due to micro-sized crystalline or defective carbons indicates vibration from the disordered terminal carbon atom. The vibration at a high frequency of 1599 cm^{1} corresponds to the G band, which is seen as a fingerprint of the graphene structure [51]. Accordingly, the G band was assigned to the inter-plane sp^2 C-C stretching. The intensity ratio of these bands (I_G/

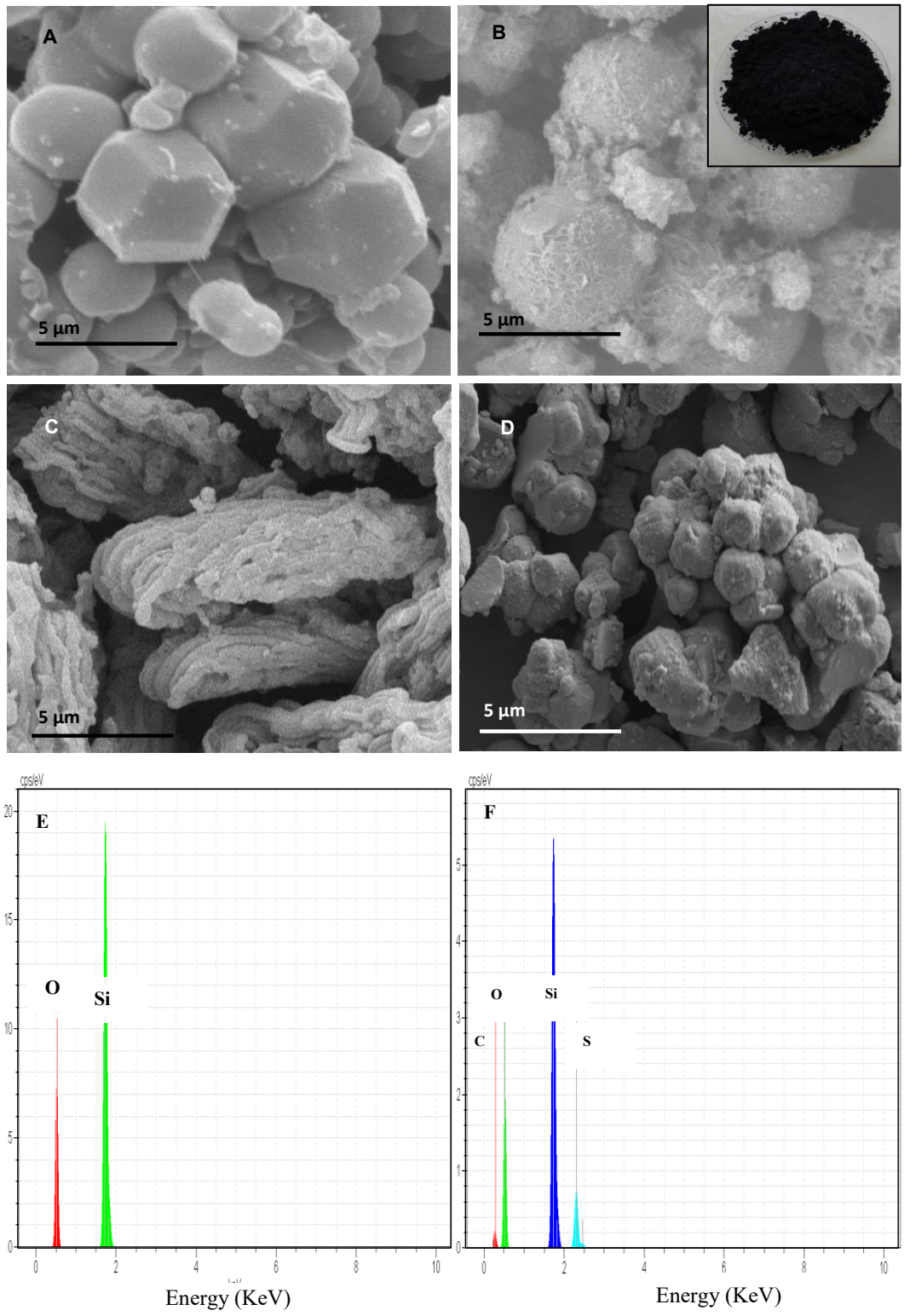

Fig. 2. Images of synthesized samples: A SEM image of ONC, B SEM image of CD-ONC, C SEM image of Au-OCMK-3, and D SEM image of SO_3H-SBA-16, and Energy dispersive X-ray spectroscopy (EDX): E SBA-16 and F SO_3H-SBA-16.

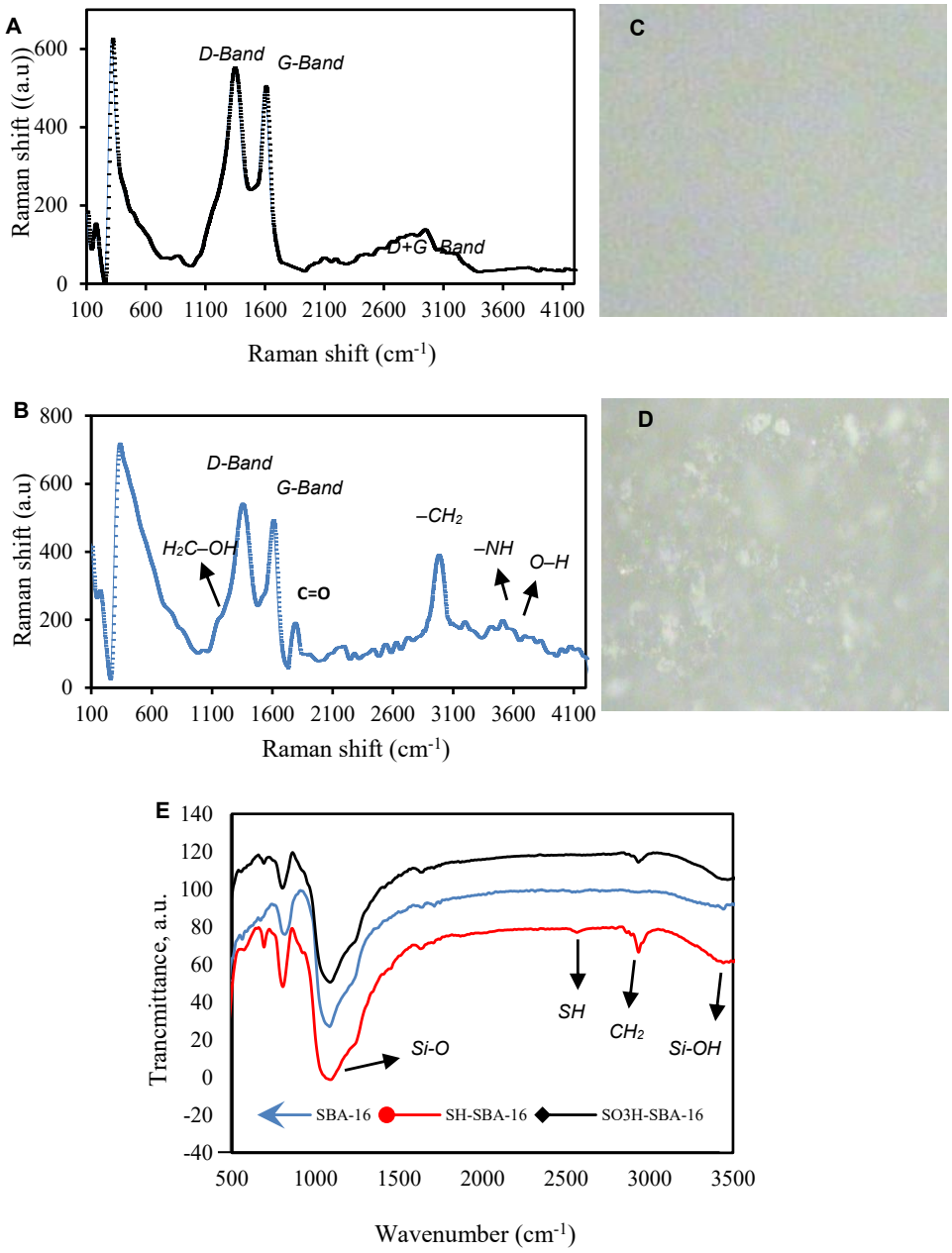

Fig. 3. A Raman spectra of ONC, B Raman spectra of CD-ONC, C Raman image of ONC, D Raman image of CD-ONC, and E FT-IR spectra of synthesized samples (SBA-16, SH-SBA-16, and SO_3H-SBA-16).

I_D) or the ratio of their areas provides significant information about the "graphicity" or the absence of defects. The ratios of the areas of *G/D* for the ONC and functionalized ONC were equal to 0.914 and 0.912, respectively. According to *G/D* intensity ratios, the unmodified mesoporous carbons appeared to be a little more graphitic than those of the CD-ONC. However, this indicated slightly further disordered structures of the CD-ONC compared to the ONC. This was more likely due to the introduction of functional groups to the mesoporous carbon. The characteristic Raman shifts [52] for grafted ONC *via* PDI (Fig. 3B) are O–H (3500 cm^{-1}), –NH (3403 cm^{-1} from urethane), $–CH_2$ (2971 cm^{-1} from β-CD), C=O in urethane (1780 cm^{-1}), G band (1599 cm^{-1} from

Table 3: The S/N ratio of each test.

Tests	Factor					PRE (%)		S/N	SD
	A	B	C	D	E	PRE_1	PRE_2		
1	60	50	20	0.3	2	32.40	33.50	30.35	0.78
2	60	100	40	0.5	4	45.00	45.01	33.07	0.01
3	60	150	60	0.7	6	52.00	51.74	34.30	0.18
4	60	200	80	0.9	10	47.00	48.30	33.56	0.92
5	120	50	40	0.7	10	50.60	50.00	34.03	0.42
6	120	100	20	0.9	6	65.00	66.00	36.32	0.71
7	120	150	80	0.3	4	33.50	33.45	30.49	0.04
8	120	200	60	0.5	2	51.50	51.35	34.22	0.11
9	180	50	60	0.9	4	55.00	56.00	34.88	0.71
10	180	100	80	0.7	2	50.00	51.00	34.06	0.71
11	180	150	20	0.5	10	54.50	54.30	34.71	0.14
12	180	200	40	0.3	6	65.50	65.35	36.31	0.11
13	240	50	80	0.5	6	46.00	45.00	33.16	0.71
14	240	100	60	0.3	10	40.00	41.00	32.15	0.71
15	240	150	40	0.9	2	65.00	64.00	36.19	0.71
16	240	200	20	0.7	4	82.00	83.00	38.33	0.71

Controllable factors: A Agitation time (min), B Concentration (mg/L), C Temperature (°C), D Dose (g/L), and E pH. PRE_1 and PRE_2 for both pollutants represent the pollutant removal efficiency at first and second test pieces, respectively. The boldfaces correspond to the maximum value of S/N ratio among the 16 tests.

ONC), D band (1344 cm-1 from ONC), and H_2C–OH (1122 cm^{-1} from β-CD). The β-CD was found as an image of white aggregates that were grafted at the surface of ONC *via* PDI, whereas the surface of ONC was seen as black regions (images of C and D in Fig. 3). We used the FT-IR technique to monitor changes on the surface of the functionalized SBA-16 with sulfonic acid groups and oxidation of thiol to sulfonic acid groups (Fig. 3E). We can attribute the absorption bands in the range of 3650–3200 cm^{-1} and 1260–1000 cm^{-1} to Si-OH and Si-O coordination. The strong peaks at 2930 cm^{-1} and 2556 cm^{-1} correspond to the asymmetric stretching of CH_2 and the stretching vibration of SH, respectively. The origin of peaks is more likely to be from $CH_2CH_2CH_2SH$ groups [53].

Taguchi's approach to the optimization of PNP adsorption

1. Analysis of variance (ANOVA)

In this study, analysis of variance was used to evaluate the optimal conditions. Equation 7 shows how to calculate the standard deviation, where $(M)_{Factor=I}^{Level=i}$ is the average S/N ratio of factor *I* at level *i*:

$$(SD)_{Factor=I}^{Level=i}=\left\{\frac{1}{n_{Ii}}\sum_{j=1}^{nIi}\left[\left(\frac{S}{N}\right)_{Factor=I}^{Level=i}-(M)_{Factor=I}^{Level=i}\right]_j\right\}^{\frac{1}{2}} \quad (7)$$

The S/N response table was prepared and the optimal conditions were obtained. Then the experiments related to these optimal conditions were performed in the laboratory. The percentage contribution of each factor [54] is calculated by Eq. (8):

$$R_F = \frac{SS_F - (DOF_R \times V_{ER})}{SS_T} \times 100 \quad (8)$$

In Eq. (8), SS_F, SS_T, and DOF_R represent the factorial sum of squares, total sum of squares, and degree of freedom of each factor, respectively. The degree of freedom for all factors is 3.

2. Performing the experiment and optimum conditions

Using Eq. (2), we calculated the *p*-nitrophenol removal efficiency for experiments 1 to 16, which results are shown in Table 3. Using the results of the measurements (PRE) and Eq. (1), the S/N ratio (Table 3). The maximum value of the S/N ratio is shown in Table 3 in boldface. $(M)_{\text{Factor=I}}^{\text{Level=i}}$ (Table 3) shows the effect of each level of each factor on the response, independently. The bold items in Table 4 refer to the values of the maximum S/N ratios of a certain factor among the four levels, which show the optimal conditions. Contact time of 180 minutes, initial concentration of 200 mg/L, temperature of 20°C, adsorbent amount of 0.9 g/L, and pH equal to 6 are the optimal conditions shown in Table 4. The PNP removal rate was checked under the mentioned conditions. The pollutant removal efficiency was calculated (91.47%) and the S/N rate was obtained using it (39.25) (Table 4). As seen, the removal conditions were improved (the average of removal was increased to 8.97 % with a 0.3 smaller standard deviation) by substantially decreasing agitation time from 240 (in Test 16) to 180 min (under the optimum conditions). In Zhao et al.'s [55] study, steel industry sludge was used as a continuous bed column for the removal of *p*-nitrophenol. The results showed that the maximum adsorption capacity was at 298 K, pH of 7, initial concentration 100 mg/L, and dose 0.8 g/L.

3. Effect of factors on the adsorption efficiency

The effect of the experimental conditions proposed by the Taguchi method is shown in Fig. 4. Fig. 4A shows the effect of agitation time on the S/N ratio. In this study, the optimal adsorbent contact time to remove phenol was 180 minutes. In explaining this event, we can say that in the early moments, there were a lot of vacant surface sites to absorb. After three hours the adsorption decreases due to the desorption process. This is a significant result because equilibrium time is one of the economic parameters in water and wastewater treatment. To investigate the effect of initial concentration on removal efficiency, different concentrations of 50 to 200 mg/L were used. Fig. 4B shows that as the concentration increases, the S/N ratio also increases. In batch experiments, it was shown that with increasing concentration, the PNP removal percentage increases. Therefore, it can be said that the removal percentage depends relatively on the initial concentration of the contaminant. Based on the experimental results, the equilibrium time for all initial concentrations was reported to be 180 minutes. In this study, we investigated the effect of temperature on the absorption of *p*-nitrophenol at temperatures of 20, 40, 60, and 80 °C. As Fig. 4C shows, with an increase in temperature of 20 to 80 ° C, the S/N ratio for the *p*-nitrophenol concentration decreases from 34.92 to 32.81. Hence, the adsorption process seems to be exothermic.

The adsorbent dose seems to be an important parameter as it determines the adsorption capacity for a given initial concentration of the contaminant [56]. The removal efficiency of PNP in different doses of 0.3 to 0.9 g/L was investigated (Fig. 4D). Experimental results show that by increasing the amount of adsorbent from 0.3 to 0.9 g/L, the removal of PNP increases. This is because as the weight of the adsorbent increases, the number of active sites increases, which in turn increases the removal of more contaminants. The highest removal efficiency of PNP was 91.47% at a dose of 0.9 g/L.

Fig. 4E shows that when pH changes from 2 to 6, the S/N ratio also increases. There are various interactions between carbon and phenol. Sometimes there are electron donor-acceptor interactions between the carbon surface and phenol. There may also be a dispersion effect between the phenolic ring and the carbon π electrons. Electrostatic attraction and van der Waals interactions are also other interactions between carbon and phenol. In the near-neutral or weakly acidic states, the three interactions of electron donor-acceptor, dispersion effects, and electrostatic attraction may occur simultaneously. In acidic conditions, the phenolic ring is adsorbed to the carbon surface through carbon π electrons [57]. The favorable physisorption of PNP to the carbonyl groups of nanoporous carbon may occur at a pH less than 6 [58]. In the electron donating-accepting mechanism of carbonyl groups, the

Table 4: S/N ratio response table for *p*-nitrophenol.

Factor/ level	$\left[(S/N)^{\text{Level=i}}_{\text{Factor=I}}\right]_j$				SD	$(M)^{\text{Level=i}}_{\text{Factor=I}}$
	j=1	j=2	j=3	j=4		
A/1	30.35	33.07	34.30	33.56	1.72	32.82
A/2	34.03	36.32	30.49	34.22	2.42	33.77
A/3	34.88	34.06	34.71	36.31	0.95	34.99
A/4	33.16	32.15	36.19	38.33	2.83	34.96
B/1	30.35	34.03	34.88	33.16	1.97	33.11
B/2	33.07	36.32	34.06	32.15	1.79	33.90
B/3	34.30	30.49	34.71	36.19	2.43	33.92
B/4	33.56	34.22	36.31	38.33	2.16	35.60
C/1	30.35	36.32	34.71	38.33	3.39	34.92
C/2	33.07	34.03	36.31	36.19	1.61	34.90
C/3	34.30	34.22	34.88	32.15	1.19	33.89
C/4	33.56	30.49	34.06	33.16	1.59	32.82
D/1	30.35	30.49	36.31	32.15	2.78	32.33
D/2	33.07	34.22	34.71	33.16	0.80	33.79
D/3	34.30	34.03	34.06	38.33	2.10	35.18
D/4	33.56	36.32	34.88	36.19	1.29	35.24
E/1	30.35	34.22	34.06	36.19	2.44	33.71
E/2	33.07	30.49	34.88	38.33	3.29	34.19
E/3	34.30	36.32	36.31	33.16	1.57	35.02
E/4	33.56	34.03	34.71	32.15	1.08	33.61

The boldface corresponds to the maximum value of the mean of the S/N ratios of a certain factor among the four levels.

Optimization results	A	B	C	D	E	PRE_1	PRE_2	SD	Mean
Test 16	240	200	20	0.7	4	82.00	83.00	0.7	82.50
Optimization condition	180	200	20	0.9	6	91.95	91.00	0.4	91.47

carbon surface acts as an electron donor, and the aromatic ring of PNP acts as an electron acceptor. At low pH (less than 3), dispersion effects are dominant. In this situation, the more polar the carbon surface is, the less PNP absorption will be, and water and PNP absorption will be competitive. At pH greater than 7, an electrostatic repulsion with the carbonyl groups of the ONC surface can be expected. In addition, the beta-cyclodextrin cavity can form a hydrogen bond with PNP [59]. In a study, Zargran et al. in 2021 [60] investigated synthesized Zn-based photocatalysts for the

Table 5. Comparing real amounts of PRE with its prediction.

Time	Con.	Tem.	Dose	pH	$(S/N)_{predicted}$	$(PRE)_{predicted}$	$(PRE)_{real}$	Error (%)	SD_{real}	$SD_{predicted}$
180	150	40	0.9	6	37.54423	75.37228	74.97	0.53	0.66	0.51
240	150	40	0.9	6	37.50639	75.04463	74.58	0.61	0.82	0.51
240	200	40	0.9	6	39.18908	91.08651	90.00	1.20	0.70	0.28

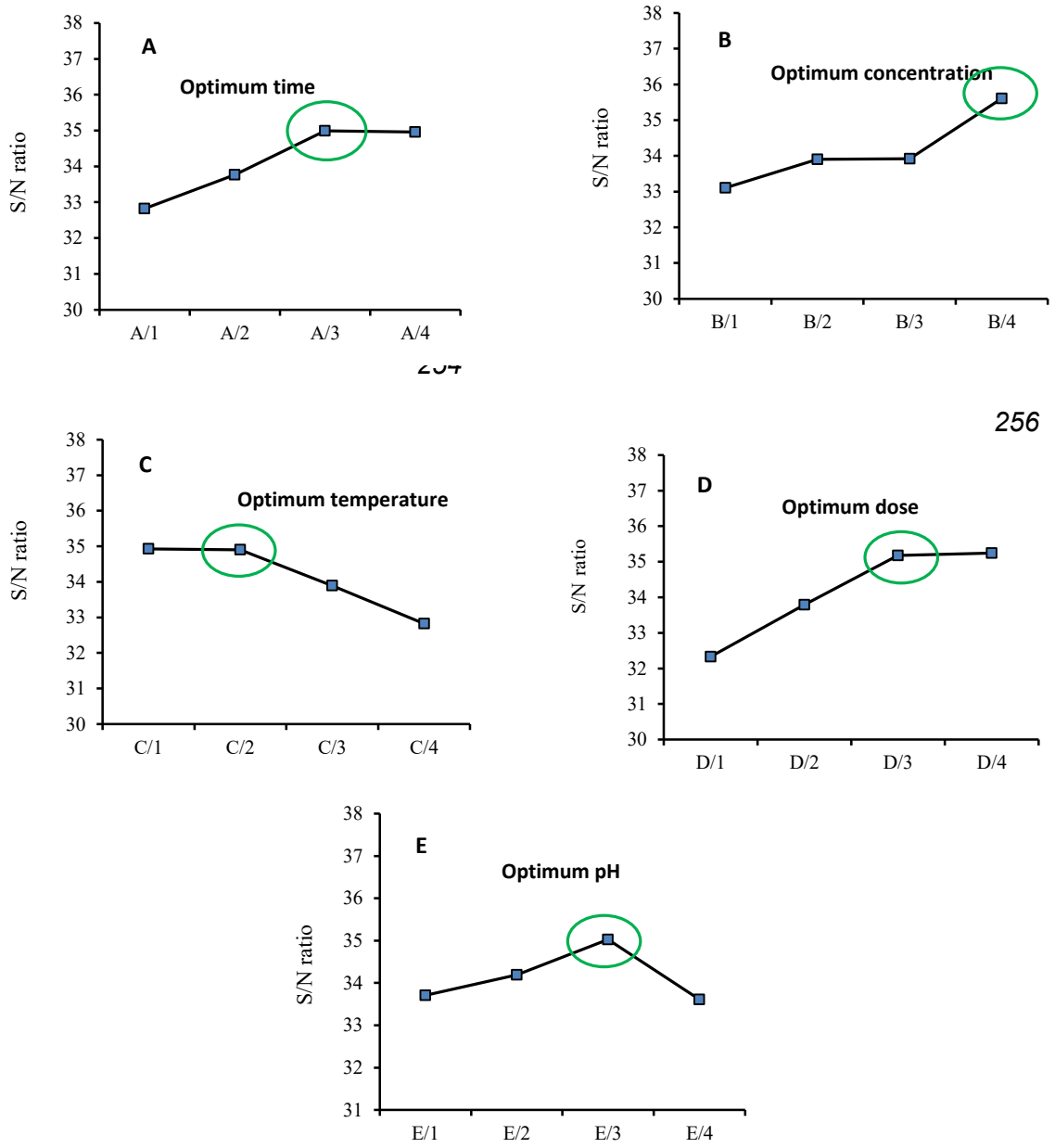

Fig. 4. The effect of time, concentration, temperature, dose, and pH on the S/N ratio for PNP adsorption onto CD-ONC. Circles on figures indicate optimum conditions for the adsorption process.

Table 6: Freundlich, Langmuir, Temkin, and Dubinin–Radushkevich parameters for adsorption of PNP on OX-ONC and CD-ONC, DBT and CA on Au-OCMK-3, and As(V) and Cu(II) on SO_3H-SBA-16.

Adsorption models	Parameters	Adsorbents					
		OX-ONC	CD-ONC	Au-OCMK-3		SO_3H-SBA-16	
				DBT	CA	As(V)	Cu(II)
Freundlich	K_f (mg/g) (L/mg)$^{1/n}$	0.02	0.18	0.17	0.16	0.01	6.24
	n (L/mg)	0.53	0.55	0.50	0.48	1.17	2.9
	R^2	0.998	0.993	0.965	0.956	0.998	0.915
Langmuir	q_m (mg/g)	83.33	100.00	15.33	13.00	92.63	43.8
	b (L/mg)	0.006	0.013	0.020	0.011	0.013	0.213
	R^2	0.950	0.966	0.998	0.995	0.951	0.991
Temkin	B (J/mol)	95.27	157.87	56.00	51.00	110.10	---
	K_T (L/g)	29.25	16.40	15.00	16.00	11.40	---
	R^2	0.904	0.902	0.913	0.911	0.901	---
Dubinin–Radushkevich	β (mol^2/J^2)	0.0004	0.0001	0.0001	0.0002	0.0001	---
	q_m (mg/g)	124.34	199.00	110.00	105.00	110.11	---
	E (KJ/mol)	0.03	0.07	0.02	0.01	0.01	---
	R^2	0.949	0.926	0.915	0.913	0.900	---

removal of Rhodamine B. The UV-Vis absorption spectrum of Rhodamine B in aqueous solution in the presence of nanocomposites showed that with an increase in irradiation time for all samples, the absorption intensity of dye at 554 nm was decreased. PH affects the pollutant degradation rate.

4. Prediction of pollutant removal efficiency

In this study, the percentage contribution of each factor, R_P, was determined. Fig. 5 shows that all parameters are important while the adsorbent dose is more important. We cannot ignore any of the factors because a contribution percentage of less than 5% can be ignored [61]. The full factorial of the tests for this study is equal to 1024 tests, of course, based on the Taguchi method, 16 tests were performed in the laboratory. Using Eq. (4), all experiments of this study (full factorial) were predicted. Also, using Table 4, the value of $(S/N)_m$ was calculated, which is equal to 34.13. Now, for example, if we consider the optimal conditions (A/3, B/4, C/1, D/4, and E/3), the value of $(S/N)_i$ for the mentioned modes are 34.99, 35.60, 34.92, 35.24 and 35.02, respectively. Equation 4 can now be rewritten as follows:

$(S/N)_{optimal}$ = 34.13 [(34.99 – 34.13) (35.61 – 34.13) (34.93 – 34.13) (35.24 – 34.13) (35.02 – 34.13)]

Therefore, the $(S/N)_{optimal}$ value is 39.25. This value can be inserted in Eq. (1) to obtain the PRE value, which was equal to 91.79%. Looking at Table 4, we can see that the estimated absorption (91.79%) is close to the real values (91.00 and 91.95) with an error of 0.34%. Fig. 5B shows the comparison of experimental errors of 16 Taguchi tests with their predicted values. Also, for better validation of Eq. (4), some other laboratory conditions were also performed, which are shown in Table 5. Total experimental error and

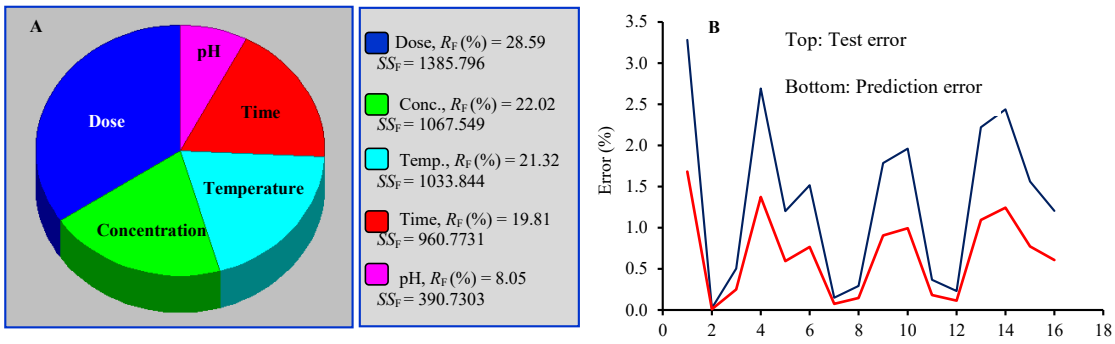

Fig. 5. A SS_F and percentage contribution of each factor, R_F and B Comparing experimental errors with its prediction.

total prediction error were 1.33% and 0.67%, respectively. Based on Table 5, it can be said that there is a good agreement between the predicted and real PRE. A comparison of the experimental standard deviation with the predicted standard deviation is also shown [36].

Equilibrium modeling for PNP adsorption on CD-ONC

1. Langmuir model

Several adsorption models have been used in this study, one of which is the Langmuir isotherm [62], which is used to obtain the maximum absorption capacity. This model shows the complete monolayer coverage on the absorbent surface as shown in Eq. (12):

$$\frac{C_e}{q_e} = \left(\frac{1}{q_m b}\right) + \left(\frac{1}{q_m}\right) C_e \qquad (12)$$

where q_e and C_e are the equilibrium concentrations of PNP in the adsorbed and liquid phases in mg/g and mg/L, respectively. To calculate the Langmuir constants (q_m (mg/g) and b (L/mg)), it is necessary to show C_e/q_e on the y-axis and C_e on the x-axis by drawing a graph. In the Langmuir model, q_m is the maximum adsorption capacity of the monolayer and b shows the adsorption affinity to the adsorption sites. The maximum absorption capacity of CD-ONC was 100 mg/g. As Table 6 shows, the absorption affinity of CD-ONC is higher than that of OX-ONC. There are two physisorption models of PNP with the surface C=O functional groups of ONC (H-bond and electrostatic repulsion).

2. Freundlich model

Another absorption model is the Freundlich model [62], which is presented in Eq. (13):

$$ln\, q_e = ln\, k_f + \left(\frac{1}{n}\right) ln\, C_e \qquad (13)$$

In the mentioned equation, k_f (mg/g)(L/mg)$^{1/n}$ and n (L/mg) show the sorption capacity and intensity, respectively. In addition, q_e indicates the equilibrium dose in the adsorbed phase in mg/g and C_e indicates the equilibrium concentration in the liquid phase in mg/L. The correlation coefficients suggest that adsorption is more compatible with the Freundlich model than other models.

3. Temkin model

The heat of absorption is reduced with the surface coverage of the adsorbent [63, 64]. Equation 14 shows the Temkin adsorption isotherm:

$$q_e = B \ln k_T + B \ln C_e \qquad (14)$$

In this equation, q_e is the absorbed amount in equilibrium (mg/g) and C_e is the absorbed equilibrium concentration (mg/L). Also, B =, (J/mol) is related to the heat of adsorption and one of Temkin's constants, R is universal gas constant (8.314 J/mol.K), T is temperature at 298K, b_T is constant of Temkin isotherm, and k_T is equilibrium binding constant of Temkin isotherm (L/g). In this study, parameter B, the adsorption energy of the Temkin equation for the adsorption of *p*-nitrophenol is positive (95.25 and 157.87 J/mol for OX-ONC and CD-ONC, respectively), which means that the adsorption is exothermic.

4. Dubinin–Radushkevich model

Dubinin–Radushkevich (D–R) isotherm describes the adsorption on both homogeneous and heterogeneous surfaces. Thus, the

Table 7: Kinetics adsorption parameters obtained using pseudo-first-order and pseudo-second-order models for the removal of PNP by CD-ONC.

Kinetics models	PNP concentration	k^*	$q_{e,cal}$ (mg/g)	$q_{e,exp}$ (mg/g)	R^2
Pseudo-first-order	50	0.0254	56.40	36.11	0.976
	100	0.0138	59.89	77.77	0.971
	150	0.0116	80.86	122.22	0.731
	200	0.0113	84.16	188.88	0.887
Pseudo-second-order	50	0.00025	47.61	36.11	0.999
	100	0.00022	95.23	77.77	0.999
	150	0.00019	116.27	122.22	0.912
	200	0.00016	129.87	188.88	0.971

*K for pseudo-first-order model is k_1 (L/min) and for pseudo-second-order model is k_2 (g/mg.min).

corresponding adsorption isotherm can be set by Eq. (15):

$$\ln q_e = \ln q_m - \beta \varepsilon^2 \quad (15)$$

where q_e is the amount of *p*-nitrophenol adsorbed onto CD-ONC (mg/g), q_m is the theoretical monolayer sorption capacity (mg/g), β is the constant of the sorption energy (mol²/J²), and ε is Polanyi potential (J²/mol²) [65], which is described as Eq. (16):

$$\varepsilon = RT \ln ( ) \quad (16)$$

In the mentioned equation, T is the temperature of the solution in Kelvin and R is the gas constant. Polanyi's theory says that there is a constant volume of adsorption sites near the surface and the adsorption potential is on these sites. The adsorption potential is related to the adsorption energy. The D–R parameter β as Eq. (17) is used to calculate the value of mean sorption energy, E (KJ/mol):

$$E = \frac{1}{\sqrt{2\beta}} \quad (17)$$

The D-R isotherm provides major information by calculating the average adsorption energy. If the absorption energy is less than 8 KJ/mol, it indicates that the physiosorption mechanism is predominant. If the adsorption energy is between 8 and 16 KJ/mol, the ion exchange mechanism is predominant. Finally, at adsorption energies higher than 16 KJ/mol, the adsorption mechanism is explained by the intraparticulate diffusion mechanism [66]. In the present study, the average free energy for OX-ONC and CD-ONC was 0.03 and 0.07 KJ/mol, respectively, indicating the existence of a physisorption mechanism.

Adsorption kinetics of p-nitrophenol

In this study, pseudo-first-order equations (Lagergren equation) and pseudo-second-order equations were used to investigate the absorption kinetics [67, 68, 69]. The Lagergren equation is $ln (q_e - q_t) = ln\, q_e - k_1 t$ (Eq. 18), here the amount of PNP absorption in mg/g at the equilibrium time with q_e, the amount of PNP absorption in mg/g at any time with q_t, and the reaction constant is introduced by k_1. Table 7 shows that the experimental q_e values are not consistent with the calculated values obtained from the linear diagram.

The pseudo-second-order kinetic equation is as follows (Eq. 19), where k_2 is the reaction constant. Table 7 shows that the adsorption of PNP onto CD-ONC follows pseudo-second-order kinetics [70].

$$\frac{t}{q_t} = \frac{1}{k_2 q_e^2} + \frac{1}{q_e} t \quad (19)$$

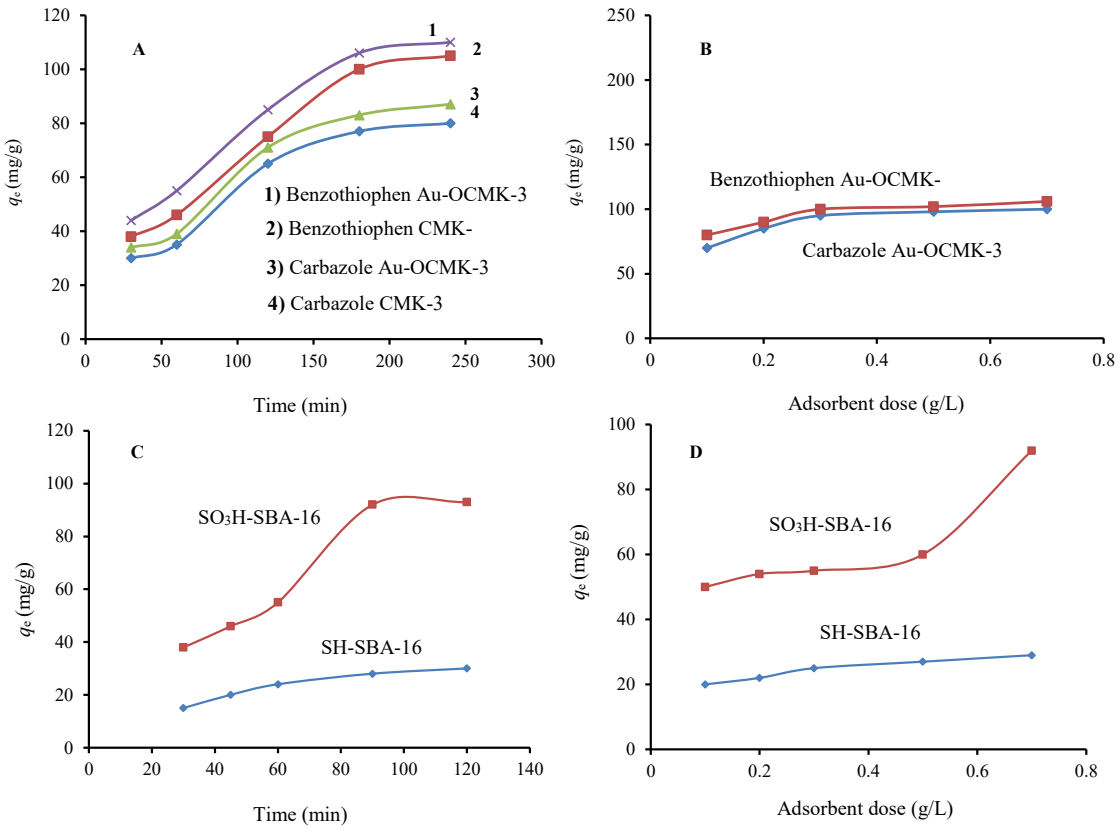

Fig. 6. The sorption of dibenzothiophene, carbazole, and arsenic on nano adsorbent studied. A Effect of Contact Time on Removal of DBT and CA (dose of 0.7 g/L and temperature of 25 °C). B Effect of adsorbent dose on the removal of DBT, CA (temperature of 25 °C for 180 min), C Effect of contact time on the removal of arsenic (dose of 0.7 g/L and temperature of 25 °C), and D Effect of adsorbent dose on the removal of arsenic (temperature of 25 °C for 90 min).

Desorption of CD-ONC

The ß-cyclodextrin on ordered nanoporous carbon was regenerated in this study using 0.1 M nitric acid. The CD-ONC was stirred with nitric acid for 2 hours at room temperature. The adsorbent and acid mixture was then filtered through the filter paper, rinsed, and dried in an oven. Having determined the amount of *p*-nitrophenol released in the aqueous solution (C_{des}) and the amount of *p*-nitrophenol adsorbed on the CD-ONC (C_{ads}), we managed to calculate the efficiency of *p*-nitrophenol recovery as follows:

$$R\,(\%) = \frac{C_{des}}{C_{ads}} \times 100 \qquad (20)$$

The regenerated CD-ONC was again used for the removal of *p*-nitrophenol at 20 °C, pH = 6, with the adsorbent value of 0.9 g/L, and over 180 minutes. This experiment was repeated 5 times. As revealed by the results, no significant reduction was found in the adsorption capacity of nanoparticles.

Thermodynamic variables

The thermodynamic variables of adsorption were calculated at a concentration of 200 mg/L, pH = 6, and the value of 0.9 g of the adsorbent, during 180 minutes at temperatures of 293, 303, and 313 °K. The thermodynamic variables such as Gibbs free energy, enthalpy changes (ΔH), and entropy changes can be examined and calculated using changes in the equilibrium constant with temperature in the equilibrium state [70]. The Gibbs free energy variation of the adsorption reaction can be calculated by the following equation:

$$\Delta G^{\circ} = -RT\ln K_d \qquad (21)$$

where ΔG°=the standard free energy changes in joules per mol, R=universal gas constant with a value of 8.31 Joule per Kelvin.mole (J/K.mol), and

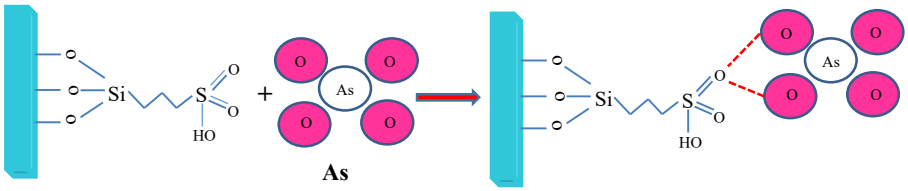

Scheme 3. Possible adsorption mechanism of As (V) onto the surface of SBA-16-SO_3H mesoporous.

T=the absolute temperature in degree Kelvin (°K). The equilibrium constant is calculated using the following equation:

K_d = The amount of heavy metal adsorbed by the adsorbent ÷ The amount of heavy metal remained in the solution × $\frac{v}{m}$ (22)

where, V=the volume of the solution in milliliters and m=the mass of the adsorbent in grams. Therefore, the standard free energy changes can be calculated by changing the temperature and measuring and calculating the equilibrium constant. On the other hand, the standard entropy changes of the adsorption and the standard enthalpy changes of the adsorption can be calculated by drawing a linear graph of the standard free energy changes with temperature with the help of Eq. (23):

$$\Delta G° = \Delta H° - T\,\Delta S° \quad (23)$$

According to the above equation, the entropy changes are calculated by drawing a linear graph of Gibbs free energy changes of the adsorption process with temperature using the slope of the line; the enthalpy changes are also calculated based on the vertical intercept (y-intercept). The Gibbs standard free energy decreased with the increased temperature. On the other hand, the variation of Gibbs standard free energy at different temperatures indicates that there is a linear behavior with a proper correlation coefficient between these two factors (R^2 = 0.99). According to Table 7, the standard enthalpy changes and standard entropy changes (ΔS°) are equal to -19055 J/mol and 6.1 (J/K.mol), respectively. The negative Gibbs standard free energy of the system indicates that the adsorption process occurs spontaneously. Also, the negative standard enthalpy changes of the adsorption reaction suggest that the process is exothermic. The positive standard entropy changes of the system also indicate an increase in irregularities in the interface of the solid/solution adsorption process.

Removal of dibenzothiophene and carbazole from oils

As mentioned earlier, this study seeks to remove hazardous substances from aqueous and non-aqueous solutions. In the following studies, the performance of other types of carbon compounds in desulfurization and denitrogenation was investigated. Removal of dibenzothiophene and carbazole was performed at different times of 30, 60, 120, 180, and 240 minutes, the results showed that the adsorption of DBT and CA on Au-OCMK-3 was higher than the CMK-3 (Fig. 6). Au species contribute to an increase in the number of active centers, improving the adsorption of DBT and CA on the mesoporous carbon. Using mesoporous Au-OCMK-3 with various doses of 0.1, 0.2, 0.3, 0.5, and 0.7 g/L in 500 mL bottles, containing 100 mL solution of 50 mg/L dibenzothiophene and carbazole, the impact of adsorbent dose on the adsorption of dibenzothiophene and carbazole was examined. The test temperature was 25°C and the contact time was 180 minutes. Using the Langmuir and Freundlich models, the q_m value for DBT was calculated as 15.33 mg/g and for CA as 13.00 mg/g. As Table 6 shows, Langmuir isotherm is more suitable than Freundlich isotherm to describe the equilibrium of DBT and CA adsorption on Au-OCMK-3. Adsorption removal of carbazole from model esterified bio-oil using metal-organic frameworks functionalized with sulfonic acid both on metal and linker sites has been investigated in the study of Abul Hossain et al. in 2023 [71]. The results of this study showed that the synthesized adsorbent has a high ability to remove carbazole.

Removal of arsenic and copper using SO_3H-SBA-16 and resorption study

The arsenic adsorption tests were done at room temperature and adsorption times of 30, 45, 60, 90, and 120 min

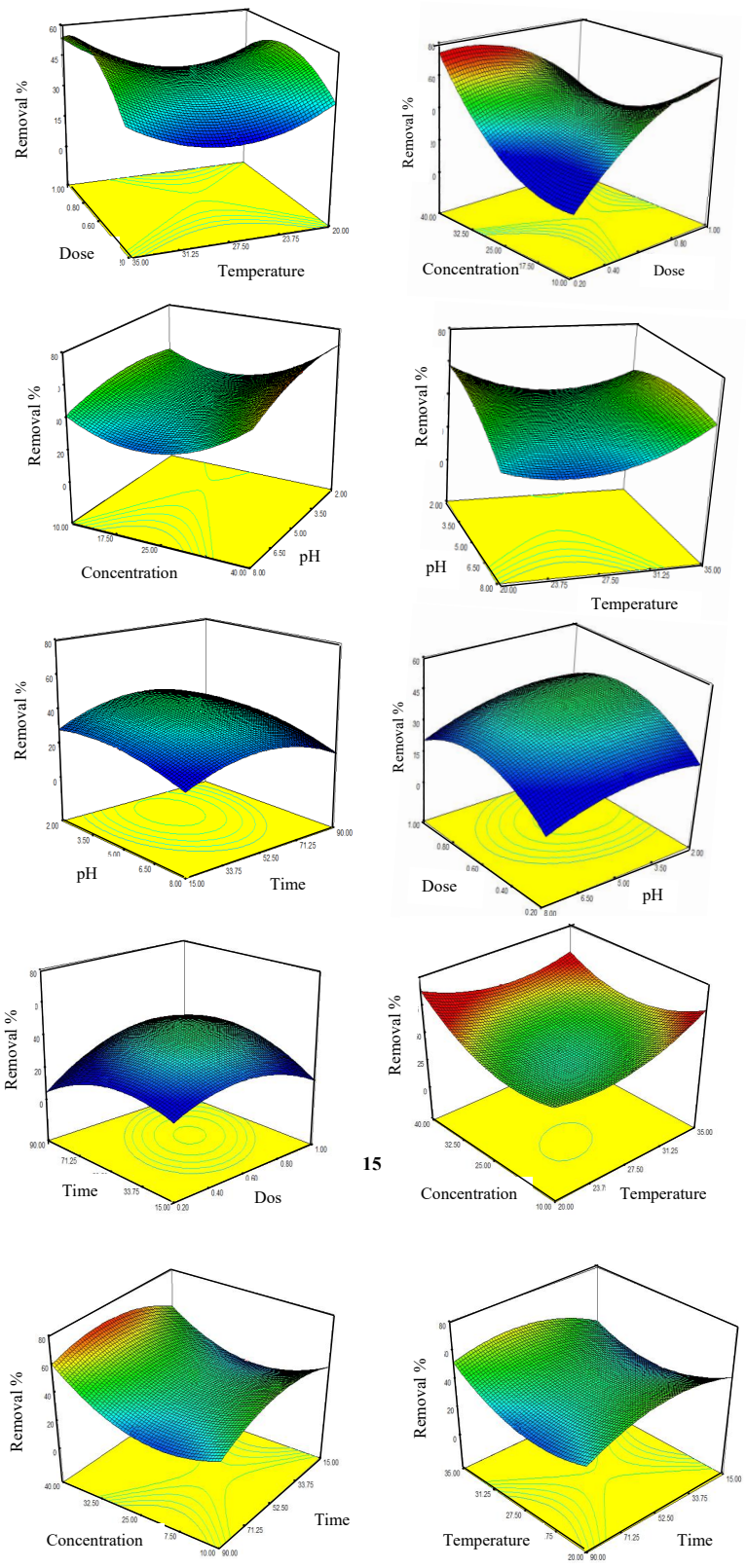

Fig. 7. Interaction effect of solution pH, concentration, temperature (°C), adsorbent dose, and contact time on copper(II) adsorption on SO_3H-SBA-16.

Table 8: Thermodynamic parameters for adsorption of PNP onto CD-ONC particles: ΔG°=the standard free energy changes, ΔH= enthalpy changes, and ΔS°= standard entropy changes.

T (°K)	K_d	ΔG° (J/mol)	ΔH° (J/mol)	ΔS° (J/K.mol)
293	1200	- 17271	-	-
303	944	-17256	-19055	6.1
313	733	-17149	-	-

(solutions concentration = 10 mg/L). The sorption of As (V) on SO_3H-SBA-16 was more than SH-SBA-16 (Fig. 6).

Different doses of adsorbent were tested to investigate the absorption rate (0.1, 0.2, 0.3, 0.5, and 0.7 g/L). Since the amount of arsenic removal with SO_3H-SBA-16 was higher than that of SH-SBA-16, it can be concluded that the functional groups on the adsorbent surface are the most important factors in the adsorption capacity. The high removal of As (V) equilibrium time of 90 minutes can be explained in terms of a strong electrostatic attraction that occurred between the SO_3H and As (V). Scheme 3 shows the possible adsorption mechanism of As (V) onto the surface of SBA-16-SO_3H mesoporous. The results of the studies of Langmuir and Freundlich isotherms show that the adsorption has better compatibility with the Freundlich model, as shown in Table 6. The results of the Temkin model for SO_3H-SBA-16 are shown in Table 6. From the linear plot of the D-R model (ln q_e versus ε^2), the mean free energy for arsenic adsorption on SO_3H-SBA-16 is equal to 0.01 KJ/mol. According to the Langmuir model, SO_3H-SBA-16 nanosorbent can remove arsenic by 92.63 mg/g. The resorption of mesoporous SO_3H-SBA-16 was studied by eluting them in different concentrations of HCL or HNO_3 (0.5 to 3 mol/L) and they were used again for adsorption. Nitric acid had better results. The maximum readsorption capacity of 92% was obtained with a 1.5 mol/L nitric acid solution. In a study conducted by Liang and Zou in 2020 on mercury adsorption with thiol-functionalized silica, the reabsorption rate was 89.6% [72]. In another study, two head-to-head comparisons were developed by Angotzi et al. [73] to highlight the As (V) adsorptive ability of mesoand macrostructured silica-based adsorbents. The results suggested that mesostructured materials are suitable for dispersing active phases as adsorbents for water treatment.

For copper adsorption on SO_3H-SBA-16, the time required to reach equilibrium was 90 minutes. A three-dimensional (3D) surface response plot was generated to investigate the effects of five process parameters, namely initial solution pH, initial Cu (II) concentration, temperature, adsorbent dose, and contact time on Cu removal. Fig. 7 shows the interaction effects of five different process variables on the response factor in the response surface plot in three dimensions. To determine the effect of dose on SO_3H-SBA-16 absorption capacity, solutions with a range of 0.2 to 1 g/L were prepared. The results show that by increasing the amount of adsorbent up to 0.7 g, the percentage of removal increased, and adding more has no effect on the removal of copper ions. In another study, it was shown that at a higher amount of adsorbent, the absorption rate was significantly improved, probably due to the increase in surface area and the availability of emptier adsorption sites. At lower amounts of adsorbent, the percentage of removal is significantly reduced due to the high ratio of copper ions to vacant sites. [74]. To determine the effect of pH on the adsorption capacity of SO_3H-SBA-16, solutions with pH between 2 and 8 were prepared. The results showed that the adsorption of copper (II) ions strongly increases with the increase of pH from 2 to 4, and remains constant with the increase of pH from 4 to 5, finally, the adsorption decreases rapidly from pH 5 to 8. At this pH value, there is a competition for adsorbent active sites between Cu (II) ions and H^+ ions from the solution. Therefore, the strong repulsive forces between the copper ion and the adsorbent lead to a decrease in the removal percentage. The sharp

decrease in absorption at a pH above 8 can be attributed to the precipitation of copper hydroxide when the pH is higher than 8. Another parameter involved in the adsorption process is temperature. It was observed that the adsorption process is also affected by temperature and the highest amount of adsorption occurred at 35 °C. The increase in removal percentage with increasing temperature may be due to the endothermic nature of the adsorption process. The effect of solution concentration on the adsorption of copper species was studied at different concentrations of 10, 17.5, 25, 32.5, and 40 mg/L of the initial solutions of the species. The results showed that the amount of adsorption increases with increasing the initial concentration of the solution. These results may be because by increasing the initial concentration, the access of the species to the active sites of the adsorbent increases and they adsorb the adsorbent faster and more. The results show that the initial adsorption rate is very fast due to the high available surface area and the adsorbent vacancies that increase the binding and driving force. RSM predicted that to achieve maximum efficiency, the optimal values for adsorbent dose, initial concentration, pH, temperature, and contact time are 0.53 g/L, 30.71 mg/L, 5.2, 25.29 °C, and 55.03 minutes, respectively. The results of the studies of Langmuir and Freundlich isotherms show that the adsorption has better compatibility with the Langmuir model, as shown in Table 6. Thirupathi et al. [16] synthesized diamino pyridyl ligand groups integrated mesoporous organosilica hybrid nanoparticles adsorbent for copper removal from aqueous solution. The results showed that the high adsorption of copper is due to the presence of many sulfonic functional groups on the mesoporous silicate wall.

CONCLUSION

The treatment of *p*-nitrophenol by cyclodextrin on ordered nanoporous carbon provided a 91.47% reduction in the PNP of aqueous solution under optimum conditions. The removal of PNP was mainly influenced by dose (28.59%), initial PNP concentration (22.02%), temperature (21.32%), and the contact time (19.81 %), and the pH had the least effect (8.05 %) on % of pollutant removal rate. One can conclude that all factors are so important and dose is more important than others. In this study, the pollutant removal efficiency was predicted by the Taguchi method. Because the overall experimental error and prediction error are respectively equal to 1.33 % and 67%, the estimates made by the Taguchi method appear to be highly acceptable. There was a good agreement between the predicted and real observed PRE, and the prediction error was almost half of the experimental error. This suggests that the Taguchi method is a very useful tool for applications in the fields of environmental engineering and industrial wastewater treatment. We demonstrate that the functionalization of CMK-3 with gold is possible. Au species contribute to an increase in the number of active centers, which improves the adsorption of pollutants on mesoporous carbon. The study results suggest that well-designed carbon-based adsorbents, for the surface area, metal ion, and surface modification, can contribute to the production of clean fuels. Langmuir coefficient q_m was 92.63 mg/g for SO_3H-SBA-16. In this approach, a high content of organic ligand functional groups could be incorporated into the silica pore walls. The SO_3H-SBA-16 adsorbent has a high complexation ability toward Cu (II) ions due to the high amount of sulfonic functional ligand groups integrated into the pore walls. For future studies, it is suggested to study the synthesized nanosorbents in a continuous column. In continuous reactors, it is possible to check the effect of flow rate and column height in a more realistic situation. The use of industrial wastewater instead of synthetic solutions in the adsorption process is important among other suggestions.

CONFLICT OF INTEREST

The authors declare that they have no known competing financial interests or personal relationships that could have appeared to influence the work reported in this paper.

ACKNOWLEDGMENTS

The authors gratefully acknowledge the Iran Nanotechnology Initiative Council. We also thank the National Elite Foundation of Iran, Vice-Presidency for Science and Technology.

REFERENCES

[1] Busca, G., Berardinelli, S., Resini, C., Arrighi, L., 2008. Technologies for the removal of phenol from fluid streams: a short review of recent developments. J. Hazard Mater. 160:265–288.https://doi.org/10.1016/j.jhazmat.2008.03.045

[2] Zolfaghari, G., 2023. The first ecological contamination study of avian mercury and lead in southeast Iran, Hamun International Wetlands. Environ. Sci. Pollut. Res. 30,

96575–96590. https://doi.org/10.1007/s11356-023-29219-9

[3] Zolfaghari, G., Esmaili-Sari, A., Ghasempouri, S.M., Faghihzadeh, S., 2007. Evaluation of environmental and occupational exposure to mercury among Iranian dentists. Sci. Total Environ. 381:59-67. https://doi.org/10.1016/j.scitotenv.2007.03.007

[4] Zolfaghari, G., Esmaili-Sari, A., Ghasempouri, S.M., Hassanzade Kiabi, B., 2009. Multispecies monitoring study about bioaccumulation of mercury in Iranian birds (Khuzestan to Persian Gulf): effect of taxonomic affiliation, trophic level and feeding habitat. Environ. Res. 109:830-838. https://doi.org/10.1016/j.envres.2009.07.001

[5] Rao, J.R., Viraraghavan, T., 2002. Biosorption of phenol from an aqueous solution by *Aspergillus niger* biomass. Bioresour. Technol. 85:165-171. https://doi.org/10.1016/S0960-8524(02)00079-2

[6] Rode, C.V., Vaidya, M.J., Jaganathan, R., Chaudhari, R.V., 2001. Hydrogenation of nitrobenzene to *p*-aminophenol in a four-phase reactor: reaction kinetics and mass transfer effects. Chem. Eng. Sci. 56:1299–1304. https://doi.org/10.1016/S0009-2509(00)00352-3

[7] Mishra, K.P., Gogate, P.R., 2011. Intensification of sonophotocatalytic degradation of *p*-nitrophenol at pilot scale capacity. Ultrason. Sonochem. 18:739–744. https://doi.org/10.1016/j.ultsonch.2010.11.004

[8] Zhao, D.M., Ding, C., Wu, C.X., Xu, X.H., 2012. Kinetics of ultrasound-enhanced oxidation of *p*-nitrophenol by Fenton's reagent. Energy Procedia. 16:146–152. https://doi.org/10.1016/j.egypro.2012.01.025

[9] Aksu, Z., Yener, J., 2001. A comparative adsorption/biosorption study of mono-chlorinated phenols onto various sorbents. Waste Manage. 21:695-702. https://doi.org/10.1016/S0956-053X(01)00006-X

Hamadi, N.K., Chen, X.D., Farid, M.M., Lu, M.G.Q., 2001. Adsorption kinetics for the removal of chromium(VI) from aqueous solution by adsorbents derived from used tyres and sawdust. Chem. Eng. J. 84:95-105. https://doi.org/10.1016/S1385-8947(01)00194-2

[10] Kuleyin, A., 2007. Removal of phenol and 4-chlorophenol by surfactant-modified natural zeolite. J. Hazard. Mater. 144:307-315. https://doi.org/10.1016/j.jhazmat.2006.10.036

[11] Pan, B.C., Zhang, X., Zhang, W.M., Zheng, J.Z., Pan, B.J., Chen, J.L., Zhang, Q.X., 2005. Adsorption of phenolic compounds from aqueous solution onto a macroporous polymer and its aminated derivative: Isotherm analysis. J. Hazard. Mater. 121:233-241. https://doi.org/10.1016/j.jhazmat.2004.10.027

[12] Farrauto, R.J., Bartholomew, C.H., 1997. Fundamentals of Industrial Catalytic Processes. Chapman and Hall, New York.

[13] Seredych, M., Bandosz, T.J., 2007. Selective adsorption of dibenzothiophenes on activated carbons with Ag, Co and Ni species deposited on their surfaces. Energy Fuels 23:3737–3744. https://doi.org/10.1021/ef900254k

[14] Alka, S., Shahir, Sh., Ibrahim, N., Ndejiko, M.J., Vo, D.N., Abd Manan, F., 2021. Arsenic removal technologies and future trends: A mini review. J. Clean. Prod. 278: 123805. https://doi.org/10.1016/j.jclepro.2020.123805.

[15] Jadoon, Z., Rauf, N.F., Syed, M., Shah, W., Naz, A., Rizwan, M., 2017. Copper in the environment: Source, environmental impact, effect on human health and remediation. 4th International Water Conference - Climate Change & Disaster Risk Management for sustainable development & Businesses. 28.

[16] Thirupathi, K., Rajesh, S., Madhappan, S., Gnanasekaran, L., Guganathan, L., Phan, T.T.V., Kim, S.C., 2023. Selective removal of copper (II) ions from aqueous solution using pyridyl-bridged mesoporous organosilica hybrid adsorbent. Environ. Res. 224: 115439-115449. https://doi.org/10.1016/j.envres.2023.115439

[17] Shokri, A., 2020. Using Mn based on lightweight expanded clay aggregate (LECA) as an original catalyst for the removal of NO2 pollutant in aqueous environment. Surf. Interfaces. 21: 100705. https://doi.org/10.1016/j.surfin.2020.100705.

[18] Shokri, A., 2021. Using NiFe2O4 as a nano photocatalyst for degradation of polyvinyl alcohol in synthetic wastewater. Environ. Chall. 5: 100332. https://doi.org/10.1016/j.envc.2021.100332.

[19] Davarpanah, M., Ahmadpour, A., Rohani Bastami, T., 2015. Preparation and characterization of anion exchange resin decorated with magnetite nanoparticles for removal of p-toluic acid from aqueous solution. J. Magn. Magn. Mater. 375: 177-183. https://doi.org/10.1016/j.jmmm.2014.09.065.

[20] Rohani Bastami, T., Khaknahad, S., Malekshahi, M., 2020. Sonochemical versus reverse-precipitation synthesis of CuxO/Fe2O3/MoC nano-hybrid: removal of reactive dyes and evaluation of smartphone for colorimetric detection of organic dyes in water media. Environ. Sci. Pollut. Res. Int. 27(9):9364-9381. doi:10.1007/s11356-019-07368-0

[21] Najafi, M., Rohani Bastami, T., Binesh, N., Ayati, A., Emamverdi, S., 2022. Sono-sorption versus adsorption for the removal of congo red from aqueous solution using NiFeLDH/Au nanocomposite: Kinetics, thermodynamics, isotherm studies, and optimization of process parameters. J. Ind. Eng. Chem. 116: 489-503. https://doi.org/10.1016/j.jiec.2022.09.039.

[22] Eizi, R., Rohani Bastami, T., Mahmoudi, V., Ayati, A., Babaei, H., 2023. Facile ultrasound-assisted synthesis of CuFe-Layered double hydroxides/g-C3N4 nanocomposite for alizarin red S sono-sorption. J. Taiwan Inst. Chem. Eng. 145: 104844. https://doi.org/10.1016/j.jtice.2023.104844.

[23] Yoon, S., Lee, J., Hyeon, T., Oh, S.M., 2000. Electric double-layer capacitor performance of a new mesoporous carbon. J. Electrochem. Soc. 147:2507-2512. https://doi.org/10.1149/1.1393561

[24] Kaneda, M., Tsubakiyama, T., Carlsson, A., Sakamoto, Y., Ohsuna, T., Terasaki, O., Joo, S.H., Ryoo, R., 2002. Structural study of mesoporous MCM-48 and carbon networks synthesized in the spaces of MCM-48 by electron crystallography. J. Phys. Chem. B. 106:1256-1266. https://doi.org/10.1021/jp0131875

[25] Ryoo, R., Joo, S.H., Jun, S., Tsubakiyama, T., Terasaki, O., 2001a. Ordered mesoporous carbon molecular sieves by templated synthesis: the structural varieties. Stud. Surf. Sci. Catal. 135:150-158. https://doi.org/10.1016/S0167-2991(01)81244-1

[26] Ryoo, R., Joo, S.H., Kruk, M., Jaroniec, M., 2001b. Ordered mesoporous carbons. Adv. Mater. 13:677-681. https://doi.org/10.1002/1521-4095(200105)13:9<677::AID-ADMA677>3.0.CO;2-C

[27] Zolfaghari, G., Esmaili-Sari, A., Anbia, M., Younesi, H., Ghasemian, M.B., 2013. A zinc oxide-coated nanoporous

carbon adsorbent for lead removal from water: optimization, equilibrium modeling, and kinetics studies. Int. J. Environ. Sci. Technol. 10:325-340. https://doi.org/10.1007/s13762-012-0135-6

[28] Vinu, A, Hossian, K.Z., Srinivasu, P., Miyahara, M., Anandan, S., Gokulakrishnan, N., Mori, T., Ariga, K., Balasubramanian, V.V., 2007. Carboxy-mesoporous carbon and its excellent adsorption capability for proteins. J. Mater. Chem. 17:1819–1825. https://doi.org/10.1039/b613899c

[29] Pluemsab, W., Fukazawa, Y., Furuike, T., Nodasaka, Y., Sakairi, N., 2007. Cyclodextrin-linked alginate beads as supporting materials for Sphingomonas cloacae, a nonylphenol degrading bacteria. Bioresour. Technol. 98:2076–2081. https://doi.org/10.1016/j.biortech.2006.08.009

[30] Can, M.Y., Kaya, Y., Algur, O.F., 2006. Response surface optimization of the removal of nickel from aqueous solution by cone biomass of *Pinus sylvestris*. Bioresour. Technol. 97:1761–1765. https://doi.org/10.1016/j.biortech.2005.07.017

[31] Taguchi, G., 1990. Introduction to Quality Engineering. McGraw-Hill, New York.

[32] Ross, P.J., 1996. Taguchi techniques for quality engineering: loss function, orthogonal experiments, parameter and tolerance design, 2nd ed. McGraw-Hill, New York.

[33] Sadrzadeh, M., Mohammadi, T., 2008. Sea water desalination using electrodialysis. Desalination 221:440-447. https://doi.org/10.1016/j.desal.2007.01.103

[34] Atile, H, Unver, Y., 2000. A different approch of experimental design: Taguchi method. Pak. J. Biol. Sci. 3:1538-1540. https://doi.org/10.3923/pjbs.2000.1538.1540

[35] Zhao, D., Feng, J., Huo, Q., Melosh, N., Fredrickson, G.H, Chmelka, B.F., Stucky, G.D., 1998a. Triblock copolymer syntheses of mesoporous silica with periodic 50 to 300 angstrom pores. Science 279:548-552. https://doi.org/10.1126/science.279.5350.548

[36] Kim, K.D., Han, D.N., Kim, H.T., 2004. Optimization of experimental conditions based on the Taguchi robust design for the formation of nano-sized silver particles by chemical reduction method. Chem. Eng. J. 104:55–61. https://doi.org/10.1016/j.cej.2004.08.003

[37] Lu, A.H., Li, W.C., Schmidt, W., Kiefer, W., Schüth, F., 2004. Easy synthesis of an ordered mesoporous carbon with a hexagonally packed tubular structure. Carbon 42:2939-2948. https://doi.org/10.1016/j.carbon.2004.07.006

[38] Bazuła, P.A., Lu, S.H., Nit, J.J., Schuth, F., 2008. Surface and pore structure modification of ordered mesoporous carbons via a chemical oxidation approach. Microporous Mesoporous Mater. 108:266–275. https://doi.org/10.1016/j.micromeso.2007.04.008

[39] Zolfaghari, G., Esmaili-Sari, A., Anbia, M., Younesi, H., Amirmahmoodi, S., Ghafari-Nazari, A., 2011a. Taguchi optimization approach for Pb (II) and Hg (II) removal from aqueous solutions using modified mesoporous carbon. J. Hazard. Mater. 192:1046–1055. https://doi.org/10.1016/j.jhazmat.2011.06.006

[40] Colilla, M., Balas, F., Manzano, M., Vallet-Regi, M., 2008. Novel method to synthesize ordered mesoporous silica with high surface areas. Solid State Sci. 10:408–415. https://doi.org/10.1016/j.solidstatesciences.2007.12.009

[41] Jun, S., Joo, S.H., Ryoo, R., Kruk, M., Jaroniec, M., Liu, Z., Ohsuna, T., Terasaki, O., 2000. Synthesis of new, nanoporous carbon with hexagonallyordered mesostructure. J. Am. Chem. Soc. 122:10712–10713. https://doi.org/10.1021/ja002261e

[42] Margolese, D., Melero, J.A., Christiansen, S.C., Chmelka, B.F., Stucky, G.D., 2000. Direct syntheses of ordered SBA-15 mesoporous silica containing sulfonic acid groups. Chem. Mater. 12: 2448-2459. https://doi.org/10.1021/cm0010304

[43] Gregg, S.J., Sing, K.S.W., 1982. Adsorption, surface area and porosity. Academic Press, London.

[44] Roy, R., A 1990. Primer on the Taguchi Method. Van Nostrand Reinhold, New York.

[45] Ayranci, E., Hoda, N., 2005. Adsorption kinetics and isotherms of pesticides onto activated carbon-cloth. Chemosphere 60:1600-1607. https://doi.org/10.1016/j.chemosphere.2005.02.040

[46] Brunauer, S., Deming, L.S., Deming, W.E., Teller, E., 1940. Theory of the van der Waals adsorption of gases. J. Am. Chem. Soc. 62:1723–1732. https://doi.org/10.1021/ja01864a025

[47] Noll, K.E., Gounaris, V., Hou, W.S., 1992. Adsorption technology for air and water pollution control. Lewis Publisher, Michigan.

[48] Zolfaghari, G., Esmaili-Sari, A., Unesi, H., Anbia, M., 2011b. Surface modification of ordered nanoporous carbons CMK-3 via a chemical oxidation approach and its application in removal of lead pollution from water. Int. Proc. Chem. Biol. Environ. Eng. 2174–2178.

[49] Kruk, M., Jaroniec, M., 2001. Gas adsorption characterization of ordered organic-inorganic nanocomposite materials. Chem. Mater. 13:3169–3183. https://doi.org/10.1021/cm0101069

[50] Zhao, D., Huo, Q., Feng, J., Chmelka, B.F., Stucky, G.D., 1998b. Nonionic triblock and star diblock copolymer and oligomeric surfactant syntheses of highly ordered, hydrothermally stable, mesoporous silica structures. J. Am. Chem. Soc. 120:6024-6036. https://doi.org/10.1021/ja974025i

[51] Dresselhaus, M.S., Dresselhaus, G., Saito, R., Jorio, A., 2005. Raman spectroscopy of carbon nanotubes. Phys. Rep. 409:47-99. https://doi.org/10.1016/j.physrep.2004.10.006

[52] Ponchel, A., Abramson, S., Quartararo, J., Bormann, D., Barbaux, Y., Monflier, E., 2004. Cyclodextrin silica-based materials: advanced characterizations and study of their complexing behavior by diffuse reflectance UV-Vis spectroscopy. Microporous Mesoporous Mater. 75:261-272. https://doi.org/10.1016/j.micromeso.2004.07.005

[53] Liang, X.F., Xu, Y.M., Sun, G.H., Wang, L., Sun, Y., Qin, X., 2009. Preparation characterization ofthiol-functionalized silica and application for sorption of Pb^{2+} and Cd^{2+}. Colloids Surf. A. 349:61–68. https://doi.org/10.1016/j.colsurfa.2009.07.052

[54] Chou, C.S., Yang, R.Y., Chen, J.H., Chou, S.W., 2010. The optimum conditions for preparing the lead-free piezoelectric ceramic of $Bi_{0.5}Na_{0.5}TiO_3$ using the Taguchi method. Powder Technol. 199:264–271. https://doi.org/10.1016/j.powtec.2010.01.015

[55] Zhao, Y., Wang, L., Zhu, L., Gao, F., Xu, X., Yang, J., 2022. Removal of p-Nitrophenol from simulated sewage using steel slag: Capability and mechanism. Environ. Res. 212, 113450-113460. https://doi.org/10.1016/j.

envres.2022.113450

[56] Aydin, H, Baysal, G., 2006. Adsorption of acid dyes in aqueous solutions by shells of bittim (Pistacia khinjuk Stocks). Desalination 196:248–259. https://doi.org/10.1016/j.desal.2005.11.025

[57] Laszlo, K., Podkoscielny, P., Dabrowski, A., 2003. Heterogeneity of polymer-based active carbons in the adsorption of aqueous solutions of phenol and 2,3,4-trichlorophenol. Langmuir 19:5287–5294. https://doi.org/10.1021/la026761s

[58] Mattson, J.S., Mark, H.B., Malbin, M.D., Weber, W.J., Crittenden, J.C., 1969. Surface chemistry of active carbon: specific adsorption of phenols. J. Colloid. Interface. Sci. 31:116-130. https://doi.org/10.1016/0021-9797(69)90089-7

[59] Schneiderman, E., Stalcup, A.M., Cyclodextrins: a versatile tool in separation science. J. Chromatogr. B. 745:83-102. https://doi.org/10.1016/s0378-4347(00)00057-8

[60] Zargarana, M., Abdoussb, M., Abdoussc, H., & Shokrid, A., 2021. Employing synthesized Zn-based photocatalysts for degradation of Rhodamine B in an aqueous environment. Desalin. Water Treat. 233: 331-340. doi: 10.5004/dwt.2021.27547

[61] Ryoo, R., Joo, S.H., Jun, S., 1999. Synthesis of highly ordered carbon molecular sieves via template-mediated structural transformation. J. Phys. Chem. B. 103:7743-7746. https://doi.org/10.1021/jp991673a

[62] Rahmanzadeh, L., Ghorbani, M., Jahanshahi, M., 2016. Effective removal of hexavalent mercury from aqueous solution by modifid polymeric nanoadsorbent. J. Water Environ. Nanotechnol. 1:1-8. https://doi.org/10.7508/jwent.2016.01.001

[63] Mittal, A., Mittal, J., Malviya, A., Gupta, V.K., 2010. Removal and recovery of Chrysoidine Y from aqueous solutions by waste materials. J. Colloid. Interface. Sci. 344:497–507. https://doi.org/10.1016/j.jcis.2010.01.007

[64] Temkin, M.J., Pyzhev, V., 1940. Recent modifications to Langmuir isotherms. Acta. Phys. Chim. Sin. 12:217–222.

[65] Itodo, A.U., Itodo, H.U., 2010. Sorption energies estimation using Dubinin-Radushkevich and Temkin adsorption isotherms. Life Sci. J. 7:31-39.

[66] Dubinin, M.M., Zaverina, E.D., Radushkevich, L.V., 1947. Sorption and structure of active carbons. I. Adsorption of organic vapors. Zh Fiz Khim (J. Phys. Chem.; English translate) 21:1351–1362.

[67] Karagoz, S., Tay, T., Ucar, S., 2008. Activated carbon from waste biomass by sulphuric acid activation and their use on methylene blue adsorption. Bioresour. Technol. 99:6214–6222. https://doi.org/10.1016/j.biortech.2007.12.019

[68] Sharma, A., Bhattacharyya, K.G., 2004. Adsorption of chromium(VI) on *Azadirachta Indica* (Neem) leaf powder. Adsorption 10:327-338. https://doi.org/10.1007/S10450-005-4818-X

[69] Robati, D., 2013. Pseudo-second-order kinetic equations for modeling adsorption systems for removal of lead ions using multi-walled carbon nanotube. J. Nanostruct. Chem. 3:55-61. https://doi.org/10.1080/1536383X.2013.787610

[70] Uslu, G., Tanyol, M., 2006. Equilibrium and thermodynamic parameters of single and binary mixture biosorption of lead (II) and copper (II) ions onto Pseudomonas putida: Effect of temperature. J. Hazard Mater. 135:87-93. https://doi.org/10.1016/j.jhazmat.2005.11.029

[71] Abul Hossain, M.D., Lee, G., Jhung, S.H., 2023. Adsorptive removal of carbazole from model esterified bio-oil composed of methyl laurate by using metal–organic frameworks functionalized with sulfonic acid both on metal and linker sites. Chem. Eng. J. 453:139822-139832. https://doi.org/10.1016/j.cej.2022.139822

[72] Liang, R., Zou, H., 2020. Removal of aqueous Hg(II) by thiol-functionalized nonporous silica microspheres prepared by one step sol–gel method. RSC Adv. 10:18534-18542. https://doi.org/10.1039/d0ra02759f

[73] Angotzi, M.S, Mameli, V., Cara, C., Borchert, K.B.L., Steinbach, C., Boldt, R., Schwarz, D., Cannas, C., 2021. Meso- and macroporous silica-based arsenic adsorbents: effect of pore size, nature of the active phase, and silicon release. Nanoscale Adv. 3:6100-6113. https://doi.org/10.1039/D1NA00487E

[74] Ghaedi, A.M., Ghaedi, M., Vafaei, A., Iravani, N., Keshavarz, M., Rad, M., Tyagi, I., Agarwal, S., Gupta, V.K., 2015. Adsorption of copper (II) using modified activated carbon prepared from Pomegranate wood: Optimization by bee algorithm and response surface methodology, J. Mol. Liq. 206:195–206. https://doi.org/10.1016/j.molliq.2015.02.029